Asteroid physical and dynamical properties from Lowell Observatory photometric database.

Dagmara Oszkiewicz[1,2,3], Ted Bowell[2],Karri Muinonen[1,4], David Trilling[3], A. Penttilä[1], T.Pieniluoma[1], L.H. Wasserman[2]

[1]University of Helsinki, [2] Lowell Observatory, [3] Northern Arizona University, [4]Finnish Geodetic Institute

Solar System science before and after Gaia
Pisa, Italy, May 4-6

Specifics of the data set:

- Lowell Observatory orbital data + MPC photometry
- MPC photometric data come from many sources
- low precision (generally rounded to 0.1 mag) and low accuracy (rms magnitude uncertainties of ± 0.2 to ± 0.3 mag are typical)
- $47,000,000$ individual, largely independent magnitude estimates
- photometric data sampled at a variety of heliocentric longitudes, and therefore asteroid spin-axis aspects
- data were calibrated using accurate broad-band photometry of asteroids observed in the course of the Sloan Digital Sky Survey (more in Oszkiewicz at al. 2011, JQSRT)

- We fit phase functions to about half a million asteroids contained in the photometric data base to obtain absolute magnitude and slope parameters.
- Relation to geometric and Bond albedo, surface porosity, packing density, roughness and grain size distribution
- Prediction of apparent magnitude

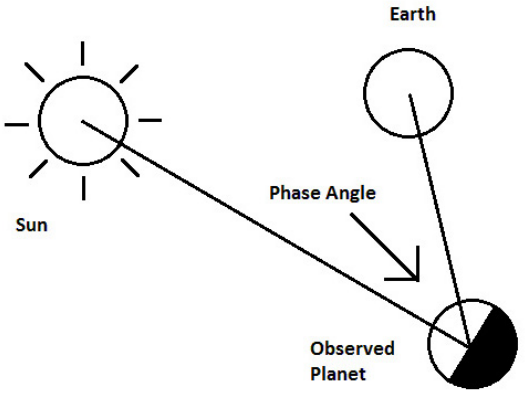

Figure: Phase angle is the angle between the light incident onto an observed object and the light reflected from the object

We made use of 3 phase functions:
The H,G phase function:

$$\begin{aligned} 10^{-0.4V(\alpha)} &= a_1\Phi_1(\alpha) + a_2\Phi_2(\alpha) \\ &= 10^{-0.4H}\left[(1-G)\Phi_1(\alpha) + G\Phi_2(\alpha)\right], \end{aligned} \tag{1}$$

The H,G_1,G_2 phase function (Muinonen et al. 2010):

$$\begin{aligned} 10^{-0.4V(\alpha)} &= a_1\Phi_1(\alpha) + a_2\Phi_2(\alpha) + a_3\Phi_3(\alpha) \\ &= 10^{-0.4H}\left[G_1\Phi_1(\alpha) + G_2\Phi_2(\alpha) + (1-G_1-G_2)\Phi_3(\alpha)\right], \end{aligned} \tag{2}$$

The H, G_{12} phase function:

$$10^{-0.4V(\alpha)} = L_0(G_1\Phi_1(\alpha) + G_2\Phi_2(\alpha) + (1 - G_1 - G_2)\Phi_3(\alpha)) \quad (3)$$

where:

$$G_1 = \begin{cases} 0.7527G_{12} + 0.06164, & \text{if } G_{12} < 0.2; \\ 0.9529G_{12} + 0.02162, & \text{otherwise;} \end{cases}$$

$$G_2 = \begin{cases} -0.9612G_{12} + 0.6270, & \text{if } G_{12} < 0.2; \\ -0.6125G_{12} + 0.5572, & \text{otherwise;} \end{cases} \quad (4)$$

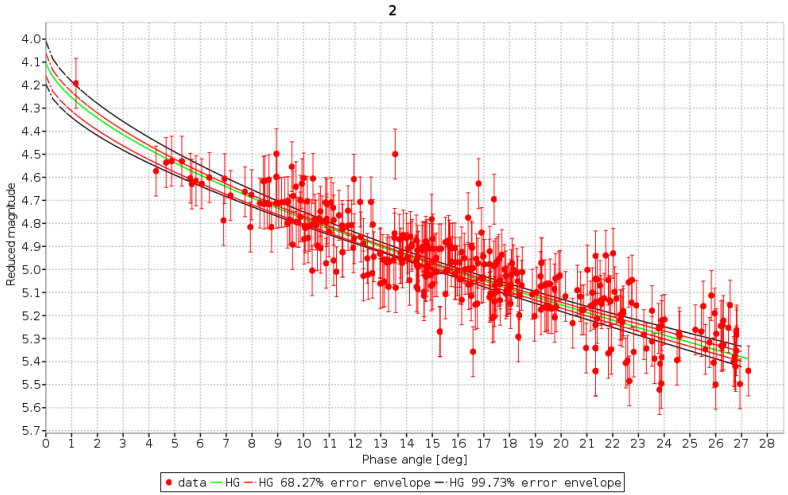

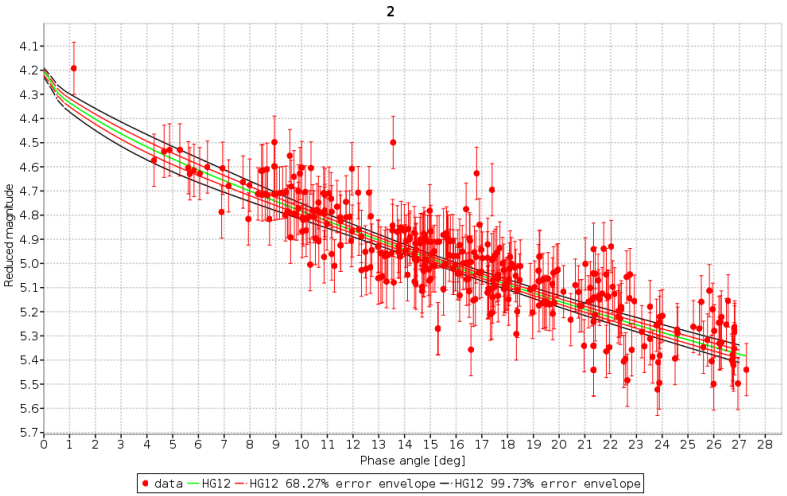

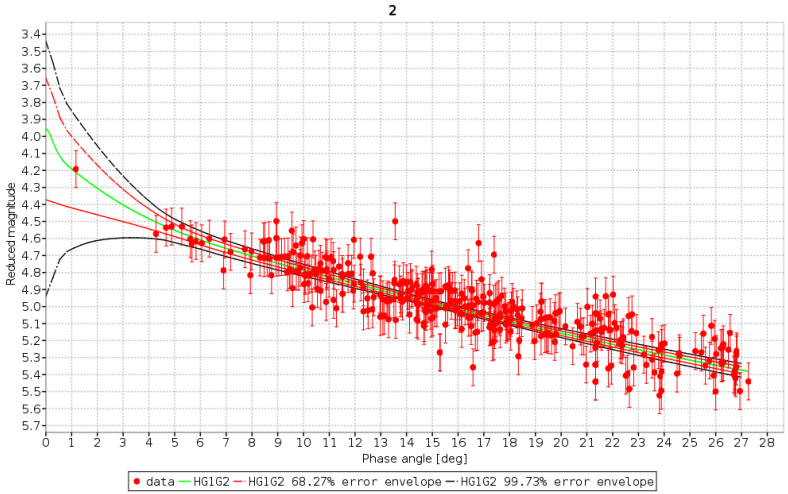

Least-squares fits to the phase curve of asteroid (2) Pallas and 68.27% and 99.73% uncertainty envelopes.

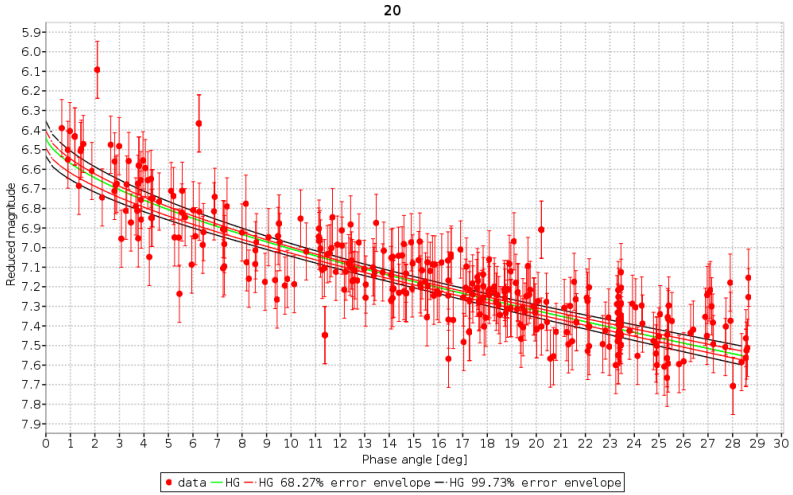

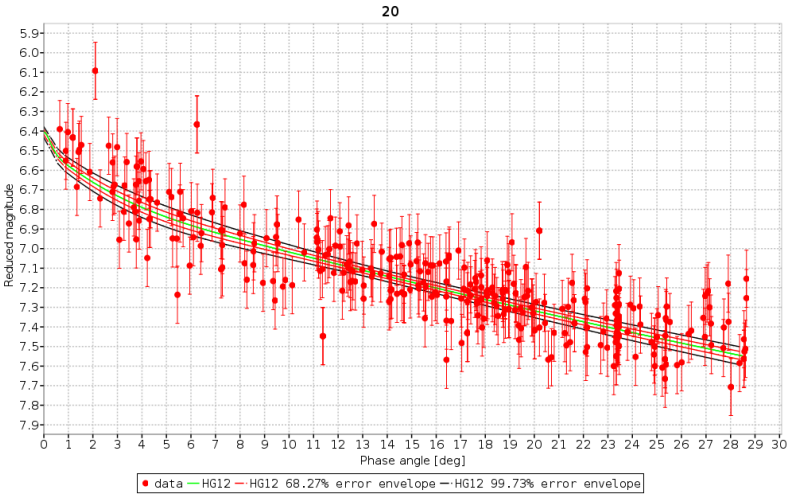

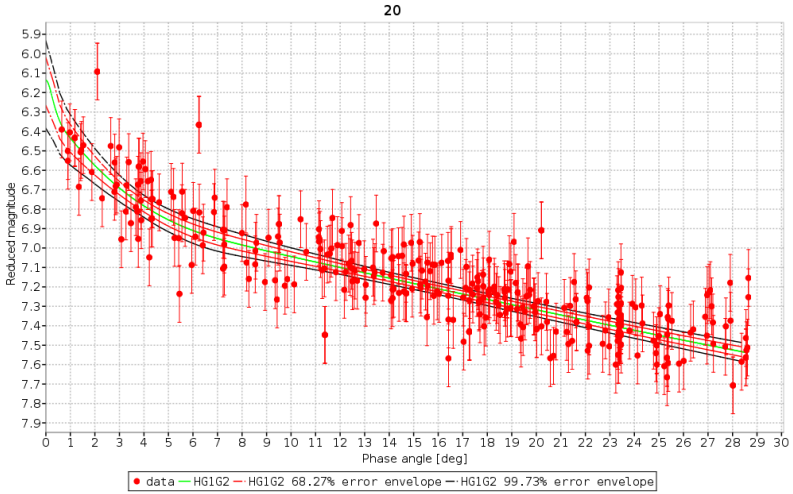

Least-squares fits to the phase curve of asteroid (20) Massalia and 68.27% and 99.73% uncertainty envelopes.

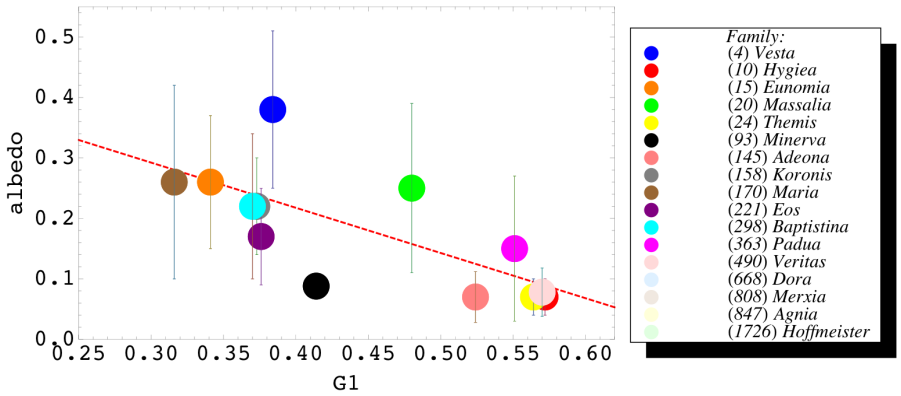

(a) Correlation between G_1 and albedo

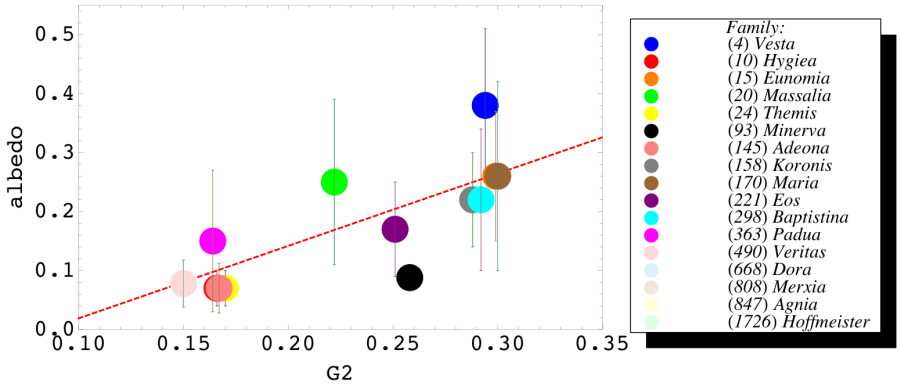

(b) Correlation between G_2 and albedo

Figure: G_1, G_2 parameters derived from the joint treatment versus albedo. Errors in G_1, G_2 are smaller than the dot size. All albedos are median family albedos except (93) Minerva, for which only parent body albedo without error estimation is available. Correlation between G_1 and albedo is -0.75 and correlation between G_2 and albedo is 0.80. Dashed line indicates linear fit to the points.

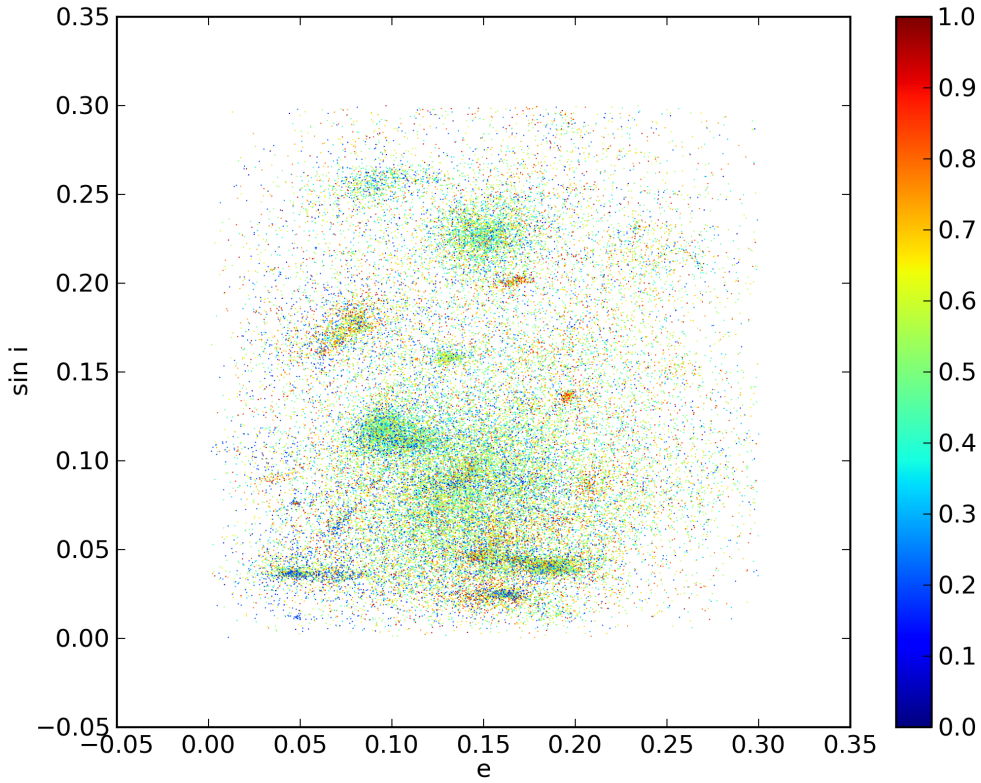

Figure: Distribution of 44, 450 asteroids with proper eccentricity, inclination defined and converged H, G_{12} solution. Dots are color coded with G_{12} values.

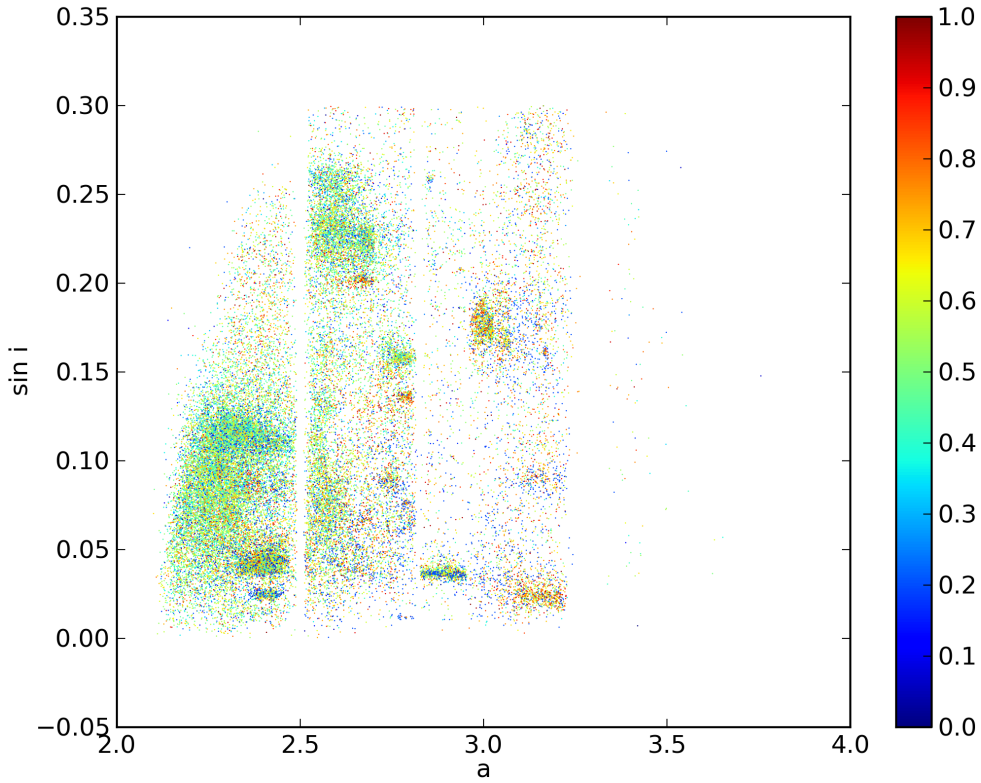

Figure: Distribution of 44, 450 asteroids with proper semimajor axis, inclination defined and converged H, G_{12} solution. Dots are color coded with G_{12} values.

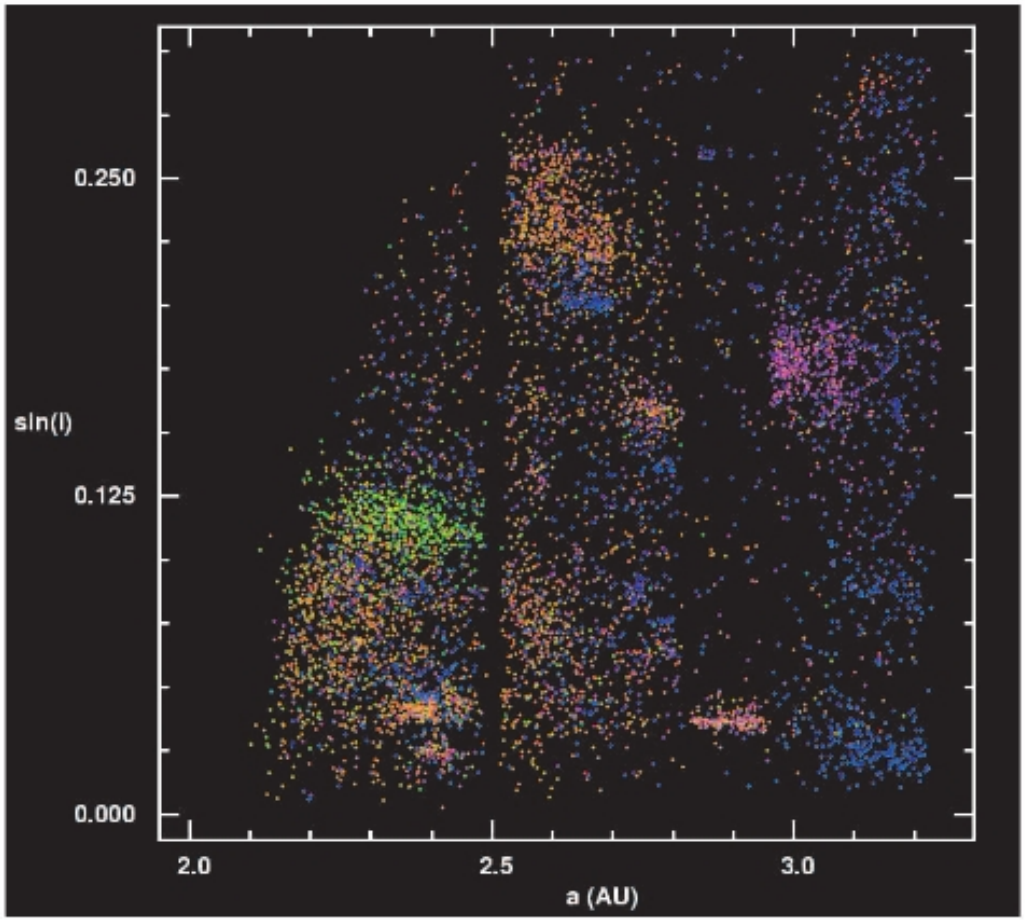

FIG. 3.—Distribution of the 6612 asteroids in the space spanned by proper inclination and semimajor axis. The dots are colored according to their position in the SDSS color-color diagram shown in Fig. 2.

From: Ivezic et al. 2002

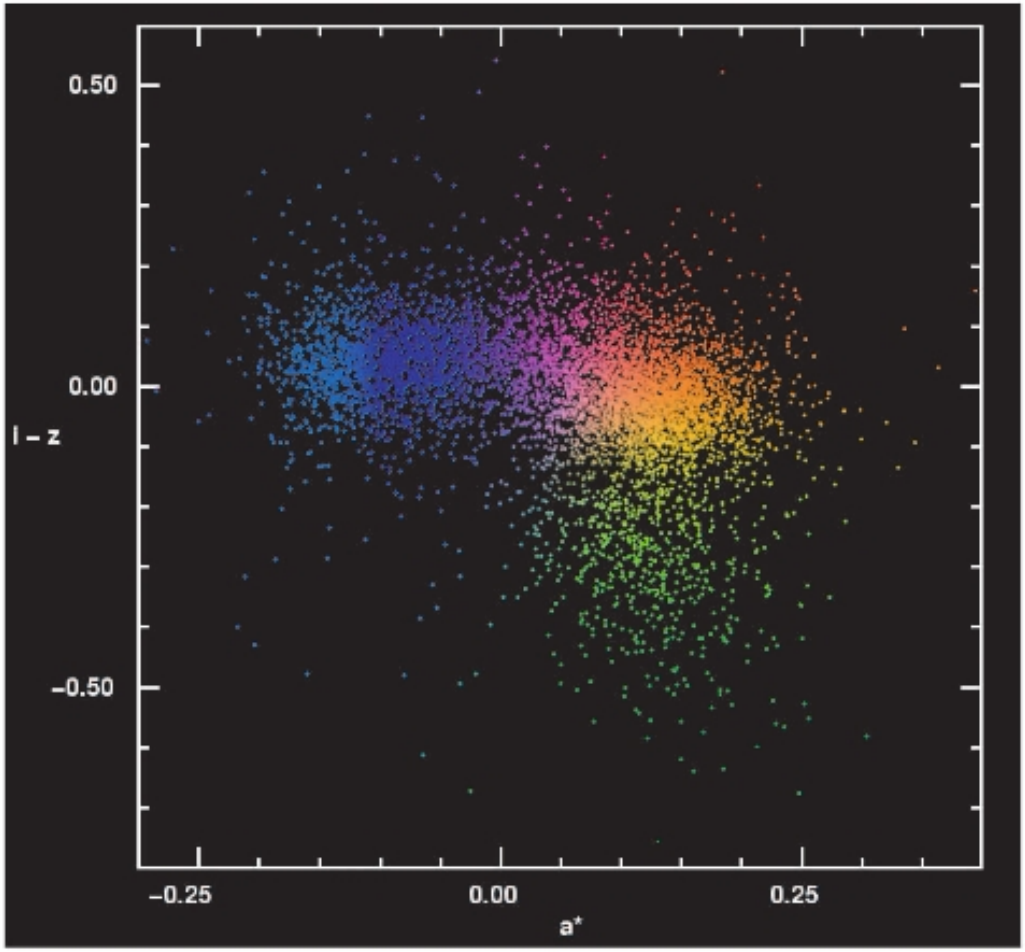

FIG. 2.—Distribution of 6612 asteroids with available proper orbital elements in the space spanned by SDSS colors

From: Ivezic et al. 2002

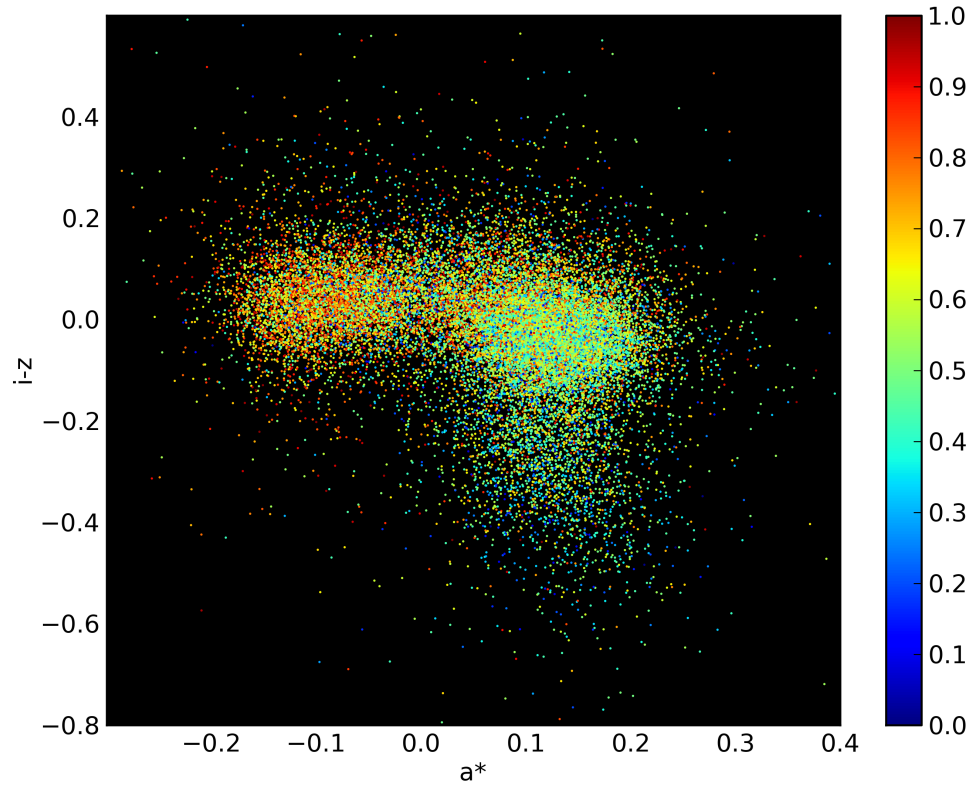

Figure: Distribution of asteroids in i-z and a* SDSS color space, color coded with G_{12} values

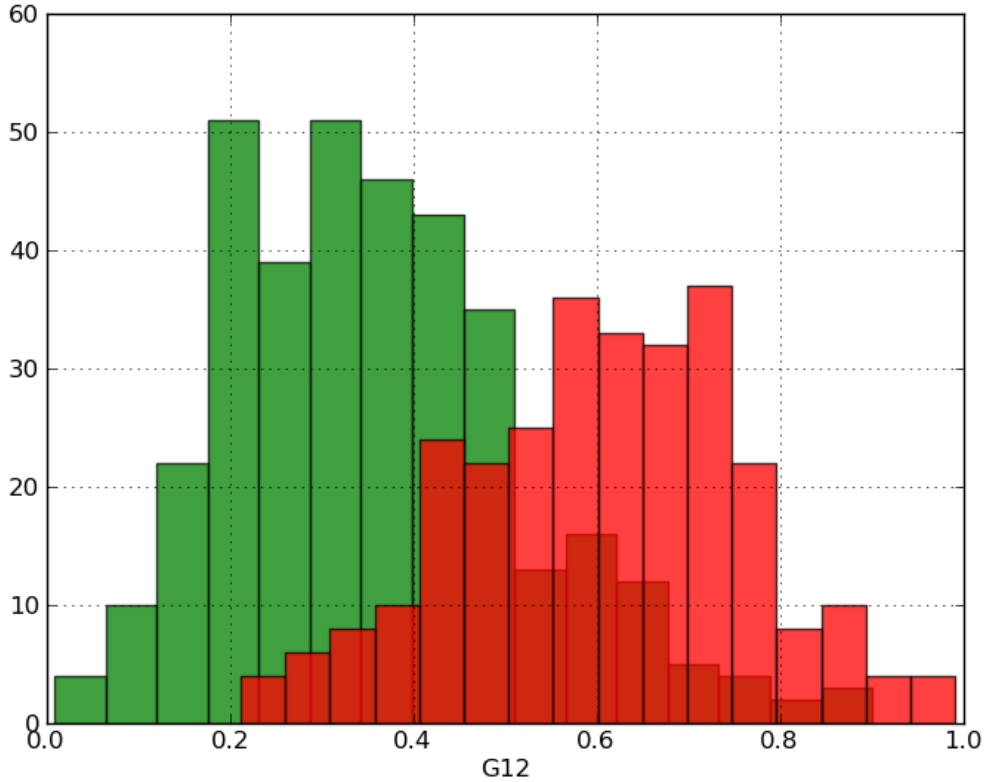

Figure: G_{12} histograms for 285 C (green) and 356 S (red) type asteroids. Diversity in composition and surface properties leads to diversity in phase curves of asteroids within the same taxonomic classification. To increase sample size asteroids of combined classes were treated as asteroids of a single class (for example, asteroids of type CG were combined with those of the predominant type C).

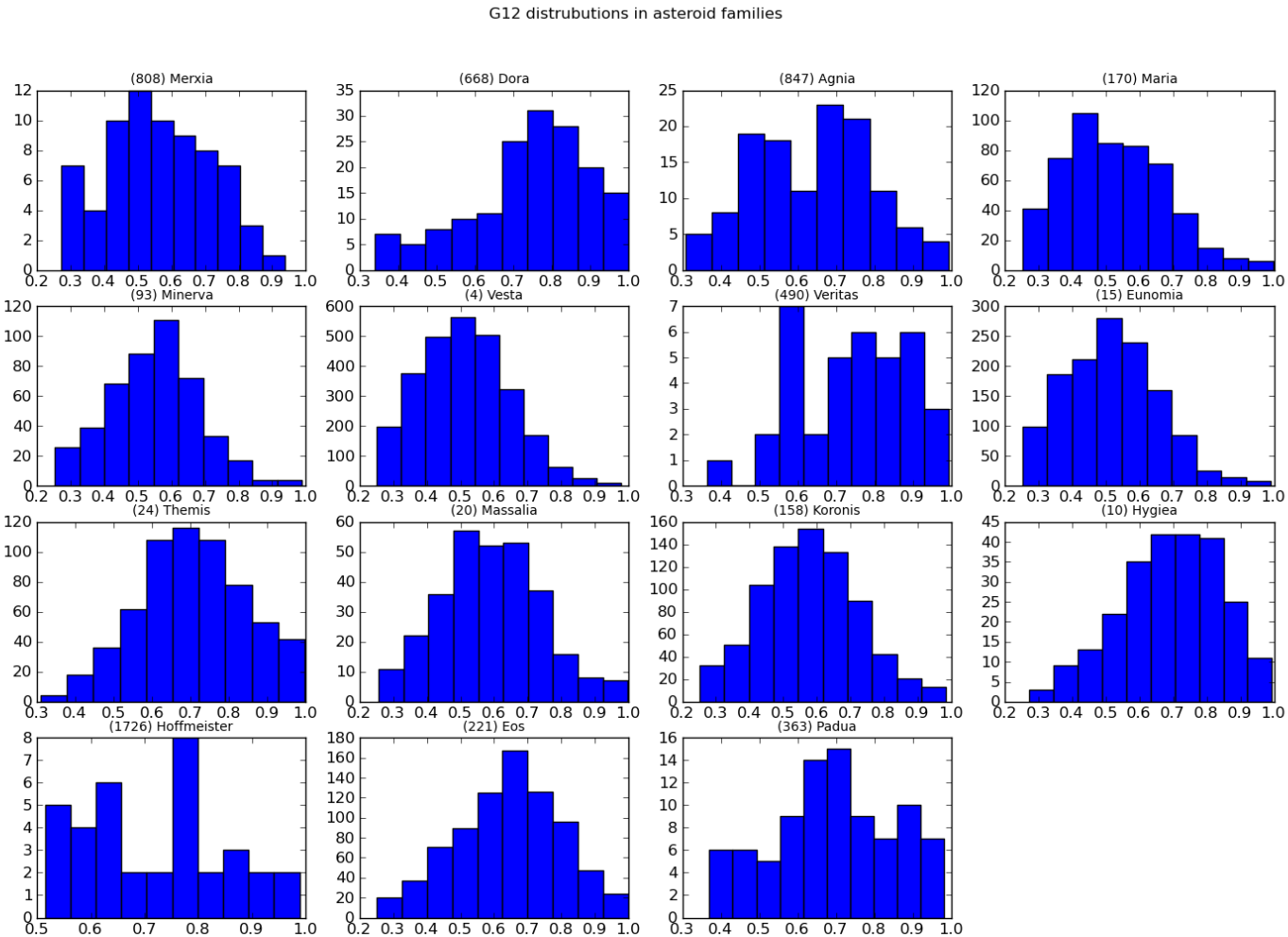

Figure: Distributions of G_{12} values in asteroid families.

Summary of phase curves fitting:

- We have produced a tabulation of photometric parameters (absolute magnitudes, slope parameters) for about half a million asteroids. We plan to propose this tabulation during the next IAU general assembly for adoption by the astronomical community,
- We found evidence for slope parameter homogeneity in asteroid families,
- Different taxonomic classes appear to have distinguishable G_{12} distributions
- Phase curve fitter: http://asteroid.astro.helsinki.fi/astphase/
- H, G_1, G_2 and H, G_{12} will be utilized in Gaia data processing pipeline

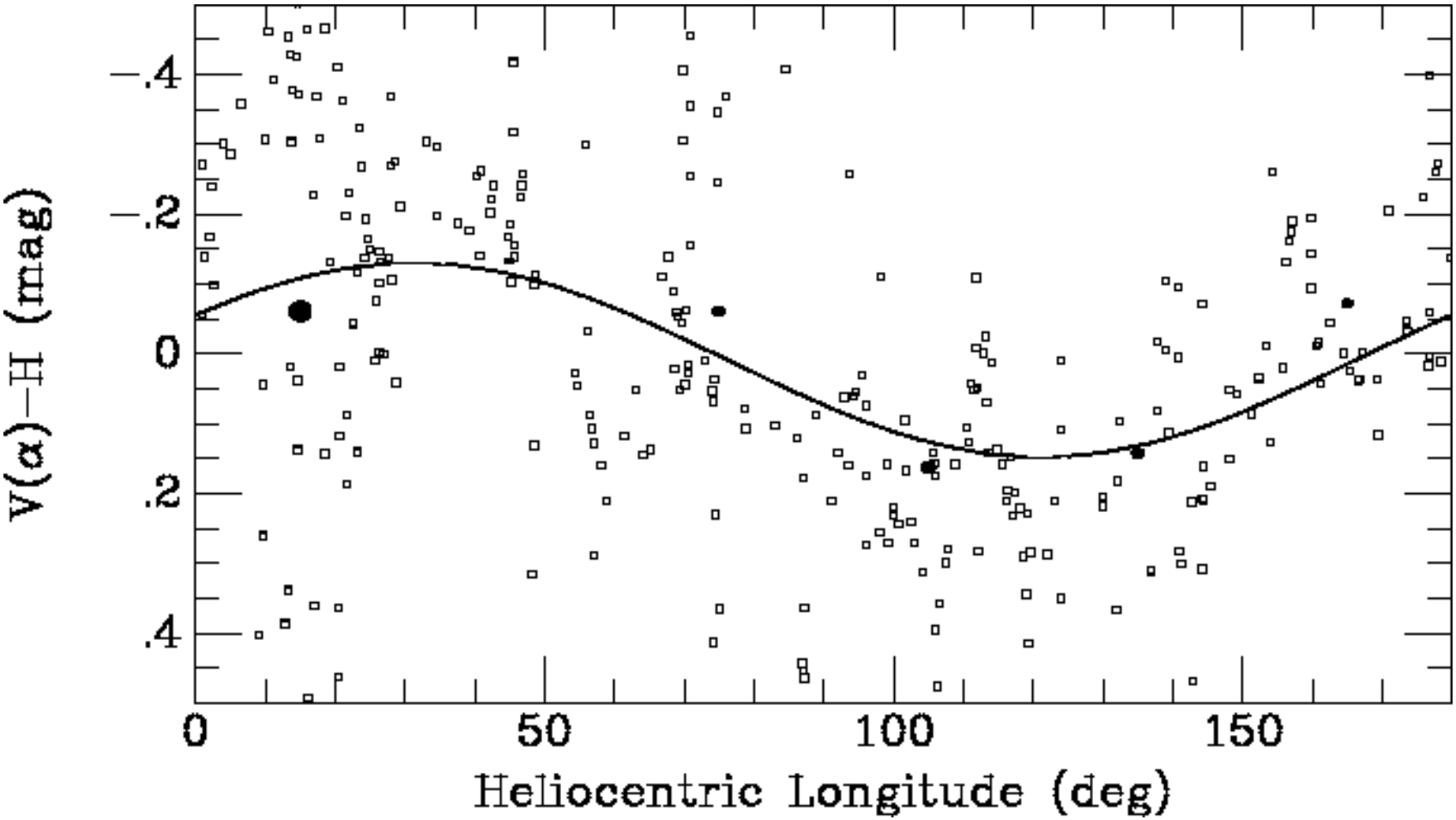

Figure: Brightness variation with heliocentric longitude for (93) Minerva.

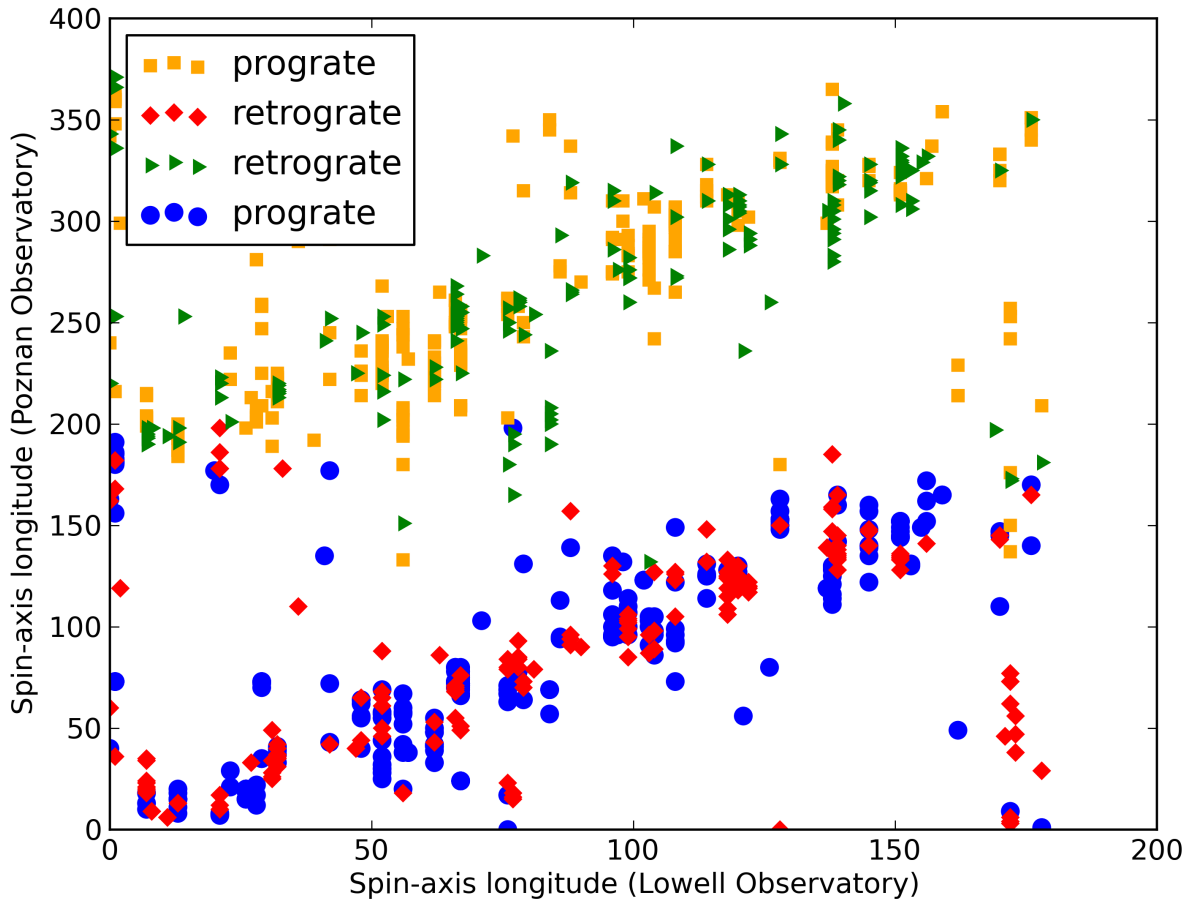

Figure: Comparison of estimations of spin-axis longitude derived based on heliocentric longitude brightness variation and on other methods.

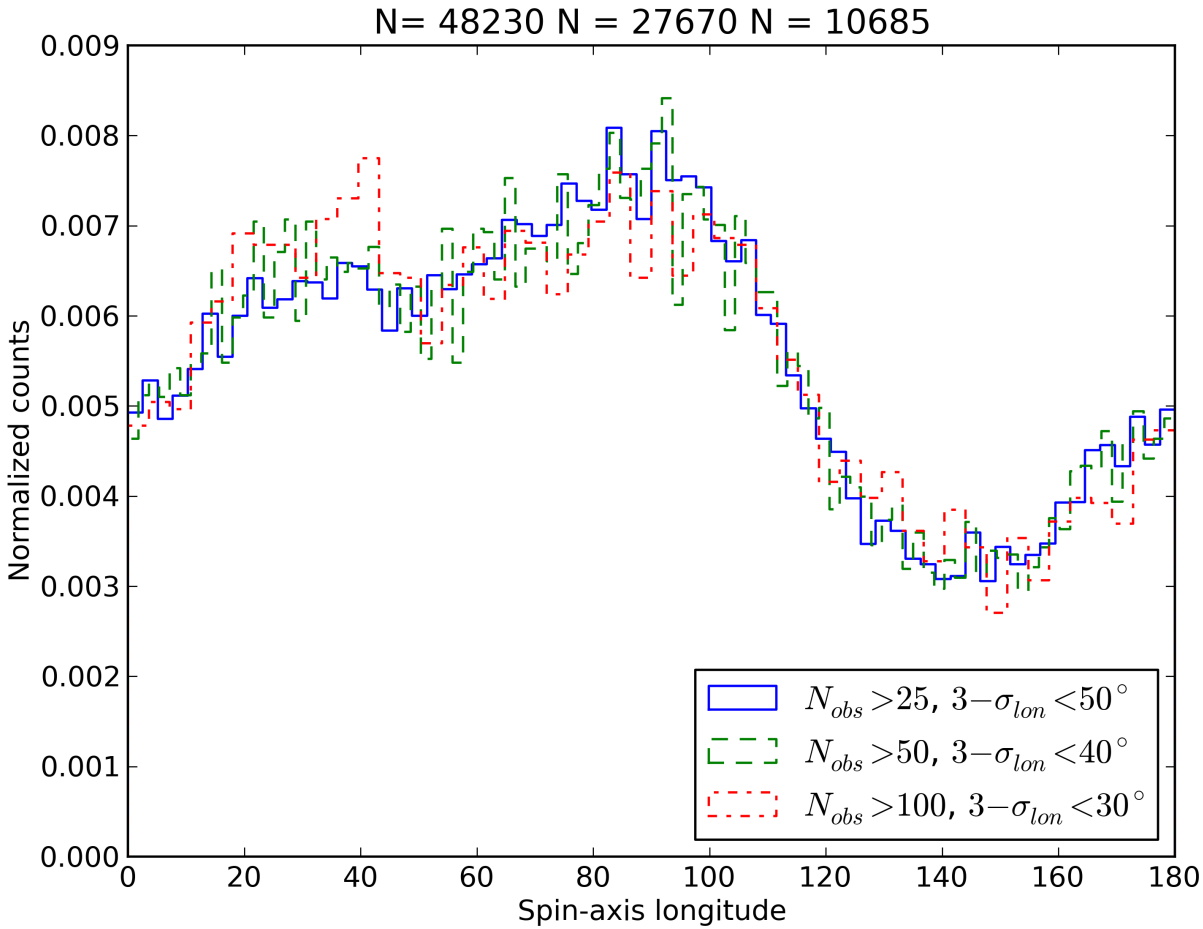

Figure: Spin-axis distribution for MBAs.

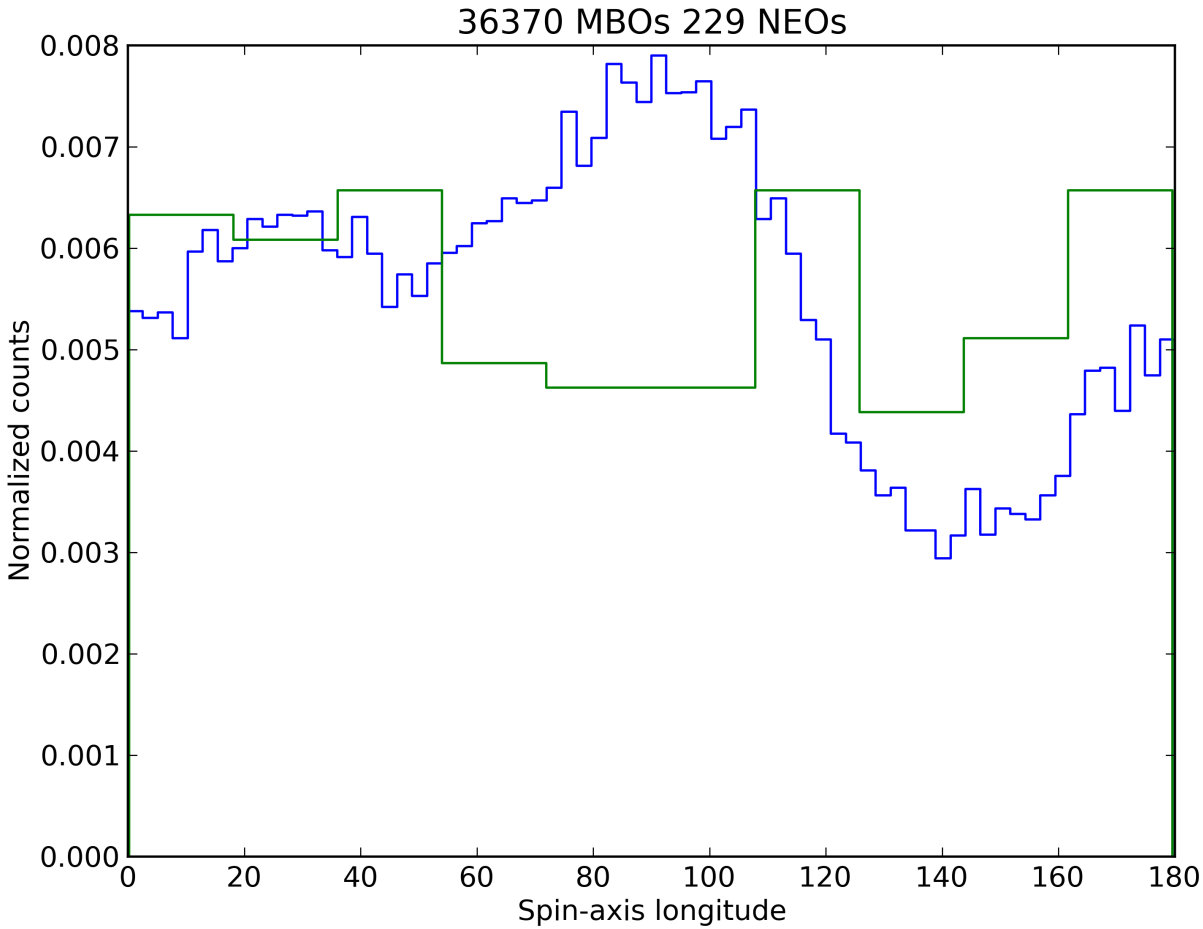

Figure: Spin-axis distribution for MBAs and NEAs.

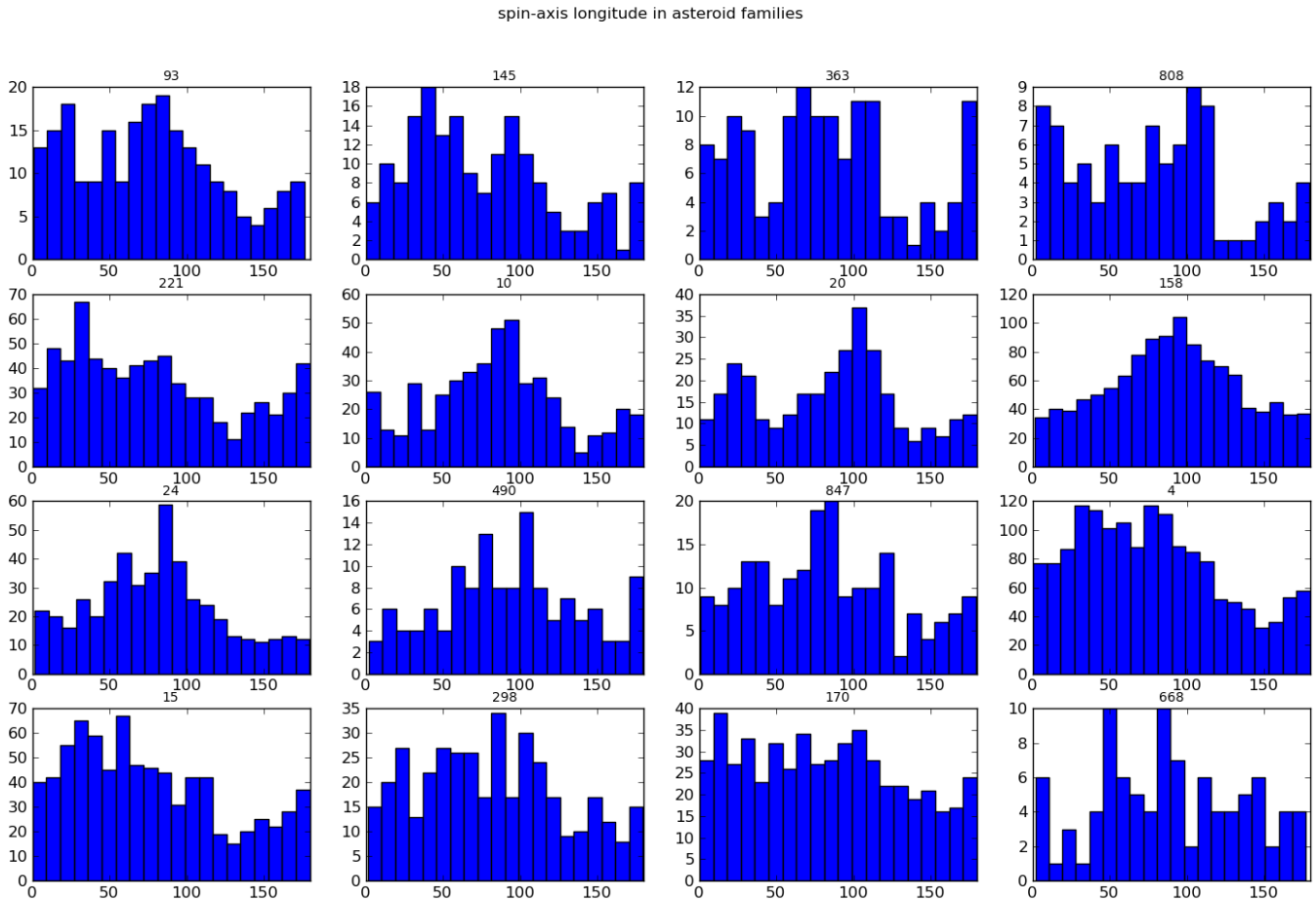

Figure: Spin-axis distribution for asteroid families.

Summary of spin-axis longitudes:

- We estimated longitudes of rotational poles for thousands of asteroids,
- We found anisotropy in spin axis-longitudes distribution for MBAs,
- Our spin-axis longitudes could help constrain phase-space of possible solutions in lightcurve inversion problem.